

Spray pyrolysis of $\text{La}_{0.6}\text{Sr}_{0.4}\text{Co}_{0.2}\text{Fe}_{0.8}\text{O}_{3-\delta}$ thin film cathodes

Journal Article**Author(s):**

Beckel, D.; Dubach, A.; Studart, André R.; Gauckler, Ludwig J.

Publication date:

2006-05

Permanent link:

<https://doi.org/10.3929/ethz-b-000025809>

Rights / license:

In Copyright - Non-Commercial Use Permitted

Originally published in:

Journal of Electroceramics 16(3), <https://doi.org/10.1007/s10832-006-6971-3>

Spray pyrolysis of $\text{La}_{0.6}\text{Sr}_{0.4}\text{Co}_{0.2}\text{Fe}_{0.8}\text{O}_{3-\delta}$ thin film cathodes

D. Beckel · A. Dubach · A. R. Studart · L. J. Gauckler

Received: 31 October 2005 / Revised: 12 December 2005 / Accepted: 28 December 2005
© Springer Science + Business Media, LLC 2006

Abstract Spray pyrolysis has been used to prepare $\text{La}_{0.6}\text{Sr}_{0.4}\text{Co}_{0.2}\text{Fe}_{0.8}\text{O}_{3-\delta}$ thin film cathodes for solid oxide fuel cell (SOFC) applications. The films are polycrystalline with nano-meter sized grains and less than $1\text{ }\mu\text{m}$ in thickness. Deposition parameters for film deposition have been established. The ratio of deposition temperature to solvent boiling point is found to be the most important processing parameter that determines whether a crack free homogeneous and coherent film is obtained. The morphology can be tailored by the deposition parameters. Annealing at 650°C for four hours in air results in coherent films of the desired perovskite phase. The films are potential cathodes for thin film micro-solid oxide fuel cells.

Keywords LSCF · Cathode · Spray pyrolysis · Thin film · SOFC

1. Introduction

Spray pyrolysis is a very versatile technique to obtain thin films of various materials and morphologies. Easy control of stoichiometry and simple experimental setup are the main advantages [1–11]. Different processes are available, which are distinguished by the method of atomizing the precursor, namely air pressurized [3, 6, 7, 11–20], electrostatic [1, 2, 4, 6, 7, 9, 18, 21–24] and ultrasonic spray pyrolysis [5, 10, 25, 26]. The method of atomization mainly determines the droplet size of the generated aerosol, which in turn determines the film quality. The film formation is also influ-

enced by the atomization method, electrostatic atomization leads to preferential landing of droplets due to their charge, a phenomenon which is not present in other atomization techniques and thus leads to unique formation mechanisms and morphologies [1, 4, 21, 23]. Even though the atomization method plays a crucial role in the spraying process, general trends are expected for some of the processing parameters such as the deposition temperature, regardless of the method of atomization. Thus for some preparation parameters comparison can be done even if the films are prepared by different atomization techniques.

The applications for thin films fabricated by spray pyrolysis are very broad, they are used as barrier layers [10, 26], for semiconductor devices such as solar cells [3, 11, 14–17, 22], sensors [3, 11, 14, 22], or photoactive layers [22]. Electrochromic materials [13, 27], catalytically active thin films [14, 16, 21] and battery components [14, 16, 21, 28] are also fabricated by means of spray pyrolysis. Solid oxide fuel cell (SOFC) electrolytes [6, 7, 18–20, 25], interconnectors [5] and cathodes [4, 9, 12, 23] have also been prepared.

SOFCs are of great interest, because of their potential to convert chemical energy into electrical energy with high efficiency. However, high operating temperatures of $800\text{--}1000^\circ\text{C}$ are required in state-of-the-art SOFC, placing heavy demands on the materials used and leading to degradation. Reliability can be increased by lowering the operating temperature, which, however, results in loss of performance. One way to improve performance at low temperatures is to use thin films as components for the SOFC [23, 25, 29], which leads to lower ohmic resistances of the single components. Indeed, SOFCs using very thin electrolytes fabricated by spray pyrolysis showed excellent performance with power densities up to 760 mW/cm^2 at 770°C [18]. The different microstructures needed for SOFC electrolytes (dense) and SOFC electrodes (porous) can be obtained using spray pyrolysis, because the

D. Beckel (✉) · A. Dubach · A. R. Studart · L. J. Gauckler
Department Materials Nonmetallic Inorganic Materials, ETH
Zürich, Wolfgang-Pauli-Str. 10, CH- 8093 Zürich, Switzerland
e-mail: daniel.beckel@mat.ethz.ch

large number of parameters involved in the spray process allows to fabricate thin films with very different microstructures. Some of the basic parameters are reported in recent work of Perednis et al. [7, 18, 30, 31]. On the other hand the amount of parameters is the challenge one faces during optimization of the process.

Most authors [1, 3, 5–8, 14, 16, 18–20, 22, 25, 28, 32–34] consider the deposition temperature to be one of the most important parameters, but no general rule for an optimum temperature has been found yet, because it also depends on the investigated materials', solvents' systems and spray pyrolysis setup. Furthermore, the literature on spray pyrolysis is also sometimes contradictory. Only limited literature is available on the preparation of $\text{La}_{0.6}\text{Sr}_{0.4}\text{Co}_{0.2}\text{Fe}_{0.8}\text{O}_{3-\delta}$ (LSCF) thin films by spray pyrolysis. Taniguchi et al. and Fu et al. [4, 23] used electrostatic spray deposition to prepare LSCF thin films. They observed different morphologies depending on the deposition temperature, composition and liquid-flow rate. The highest porosity was found for the lowest investigated deposition temperature (250°C) [23]. However, porosity was mainly restricted to the surface of the film, the lower part was rather dense. Fu et al. [4] on the other hand observed an increase of porosity with increasing deposition temperature. Very porous layers with fractal structure were obtained. However, it is not reported if they are still coherently enough to exhibit reasonable conductivity. Both authors used different solvent systems, which may explain the contradicting results. To our knowledge, no literature exists on air-pressurized spray pyrolysis of LSCF thin films, which will be the subject of this work. This paper reports on the influence of the preparation parameters on LSCF thin films fabricated with an air-pressurized spray pyrolysis process and suggests a model of the formation of these films. The aim is also to establish guidelines to prepare these films which may be valid also for other systems in order to facilitate fabrication of thin films by spray pyrolysis.

2. Experimental

2.1. Film preparation

All films are prepared by air pressurized spray pyrolysis. The metal salts are dissolved in a solvent mixture. The solution is pumped (peristaltic pump: Ismatec MS Reglo or syringe pump: Razell Scientific Instruments A 99) using a viton tube (Masterflex/Cole-Parmer) through a nozzle (Badger Air-brush Model 150) and atomized by adjustable (EAR 2000 F 02, SMC, and Norgren/IMI) air pressure. The formed droplets are sprayed onto a heated substrate (custom made heating plate with temperature precision of $\pm 1^\circ\text{C}$ in the deposition area) where an amorphous metal-oxide film

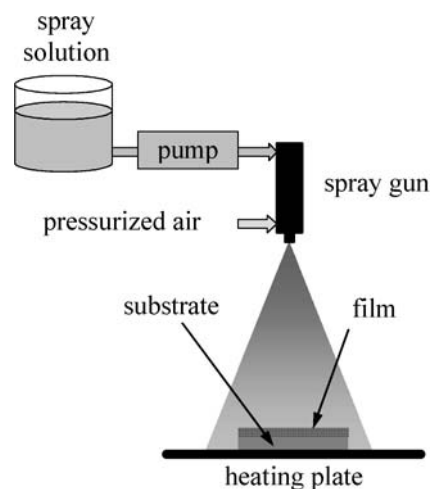


Fig. 1 Sketch of the air pressurized spray pyrolysis setup

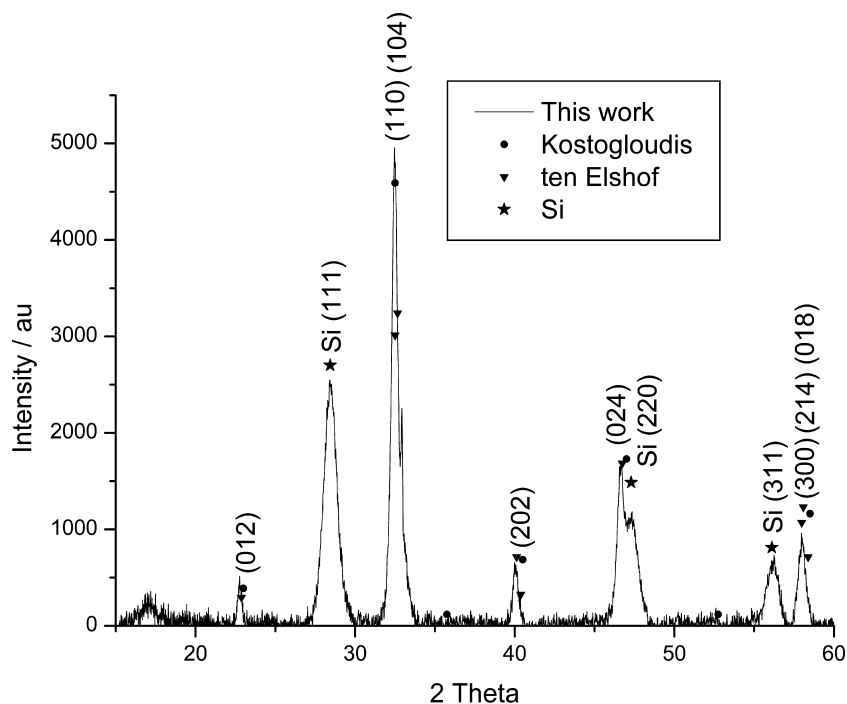
is formed, as shown schematically in Fig. 1. In an additional annealing step the films can be crystallized (Nabertherm L 3 oven).

Silicon, sapphire, and glass are used as substrates. The thermal expansion coefficient (TEC) varies from $3.6 \cdot 10^{-6}/^\circ\text{C}$ for silicon [35], $8.1 \cdot 10^{-6}/^\circ\text{C}$ for sapphire [35] to $8.6 \cdot 10^{-6}/^\circ\text{C}$ for the glass [36]. Despite this difference in TEC, no influence of the substrate material on the film morphology is found. The standard conditions for sample preparations are: At a deposition temperature of the substrate of $255 \pm 5^\circ\text{C}$ (measured with a handheld surface probe of type K, Omega Model 88108), the droplets are deposited at an air pressure of 1 bar with a solution flow rate of 30 ml/h, using a nozzle to substrate distance of 20 cm. In general, a spraying time of 60 min is sufficient for a layer thickness of ~ 700 nm. For the spray solution, a mixture of salts with a molar ratio of $\text{LaNO}_3 \cdot 6\text{H}_2\text{O} : \text{SrCl}_2 \cdot 6\text{H}_2\text{O} : \text{Co}(\text{NO}_3)_2 \cdot 6\text{H}_2\text{O} : \text{Fe}(\text{NO}_3)_3 \cdot 9\text{H}_2\text{O} = 3:2:1:4$ (all from Fluka with purity >98 or 99%) and a total salt concentration of 0.02 mol/l was dissolved in a solvent composition of 1/3 (volume fraction) ethanol (Scharlau and Merck, purity > 99.5%, boiling point 78°C) and 2/3 diethylene glycol monobutyl ether (from Fluka and Acros Organic, purity 98 and 99%, boiling point 231°C). The post deposition annealing conditions are chosen to be 4 hrs at 650°C in air with a heating ramp of $3^\circ\text{C}/\text{min}$. In the results section, preparation details are only given if they deviate from the standard parameters given above.

2.2. Film characterization

The droplet volume distribution during spray pyrolysis is measured near the nozzle using a laser deflection spectrometer (Sympatec Helos KF). The adhesion of the films to the substrate is checked by sticking a scotch tape to the film and removing it. The films show very good adhesion, because no trace of the film is found on the tape after removing.

Fig. 2 XRD pattern of an LSCF thin film deposited on silicon showing the desired rhombohedral perovskite. The film was annealed at 650°C for 4 h. References for the same composition ($\text{La}_{0.6}\text{Sr}_{0.4}\text{Co}_{0.2}\text{Fe}_{0.8}\text{O}_{3-\delta}$) from Kostogloudis [39] and ten Elshof [37] as well as for the substrate [40] are also shown



Morphology is investigated using scanning electron microscopy (SEM, Leo 1530). The roughness of the films is measured with a profilometer (Hommel Tester T1000 LV15).

Determination of the crystal phase is done by X-ray diffraction (XRD, Bruker AXS D8 Advance) on the thin films deposited on silicon substrates. The substrate can still be detected and is used as a calibration standard. After annealing of 4 hrs at 650°C in air, crystalline films of the desired rhombohedral perovskite are obtained, as shown in Fig. 2. The hexagonal lattice parameters of $a = 5.51 \text{ \AA}$ and $c = 13.51 \text{ \AA}$ are in good agreement with literature data obtained for a powder of the same stoichiometry: $a = 5.51 \text{ \AA}$, $c = 13.39 \text{ \AA}$ [37].

3. Results and discussion

3.1. Ratio of deposition temperature to solvent boiling point

Depositing an LSCF film, using the standard parameters described in the experimental section, results in a coherent crack-free film as shown in Fig. 3A. In this case the deposition temperature (T_{dep}) is 255°C and the solvent boiling point (T_{sbp}) is 180°C, thus the ratio of $T_{\text{dep}}/T_{\text{sbp}}$ equals 1.17 (in K). For these single phase solvent mixtures we simply take a solvent boiling point reflecting the composition of the solvent by $T_{\text{sbp}} = 1/3 T_{\text{bpEthanol}} (78^\circ\text{C}) + 2/3 T_{\text{bpDiethyleneGlycolMonobutylEther}} (231^\circ\text{C}) = 180^\circ\text{C}$. Even if equilibrium evaporation data, such as lower or upper boiling point would be available, it would not apply here, due to the fast evaporation during the spray

pyrolysis process. Thus we take this easy accessible temperature to establish this empirical guideline which correctly describes our experimental data.

Fig. 3B shows a film deposited at 225°C. To maintain the same ratio of $T_{\text{dep}}/T_{\text{sbp}}$, the solvent boiling point is lowered by increasing the ethanol content in the solvent from 1/3 to 1/2. The film is still coherent and crack-free and shows a smoother surface. Fig. 3C shows a film which is again deposited at the same $T_{\text{dep}}/T_{\text{sbp}}$, but the absolute deposition temperature is only 195°C. The ethanol content of the solvent is increased even further to 2/3 to keep the ratio $T_{\text{dep}}/T_{\text{sbp}}$ constant by lowering the solvent boiling point to 129°C. Also in this case, the film is coherent and crack free with an even smoother surface. As shown in Fig. 3A to C, when the ratio $T_{\text{dep}}/T_{\text{sbp}}$ is constant, crack-free coherent films are obtained independently of the absolute deposition temperature. However, the roughness of the films changes with the solvent composition.

For a lower $T_{\text{dep}}/T_{\text{sbp}}$ ratio of 1.02, the film shows cracks developing perpendicular to the surface, as exemplified in Fig. 3D for a deposition temperature of 190°C and the standard solvent composition with 1/3 ethanol. Fig. 3E on the other hand shows a film deposited at 320°C with the same solvent composition, corresponding to a ratio of $T_{\text{dep}}/T_{\text{sbp}} = 1.31$. In this case no continuous film is obtained, but irregular deposits which do not cover the substrate completely. In the present work, coherent crack-free films are obtained for $1.15 < T_{\text{dep}}/T_{\text{sbp}} < 1.25$, as schematically shown Fig. 3F. Furthermore, faster film deposition is observed for smaller $T_{\text{dep}}/T_{\text{sbp}}$ ratios.

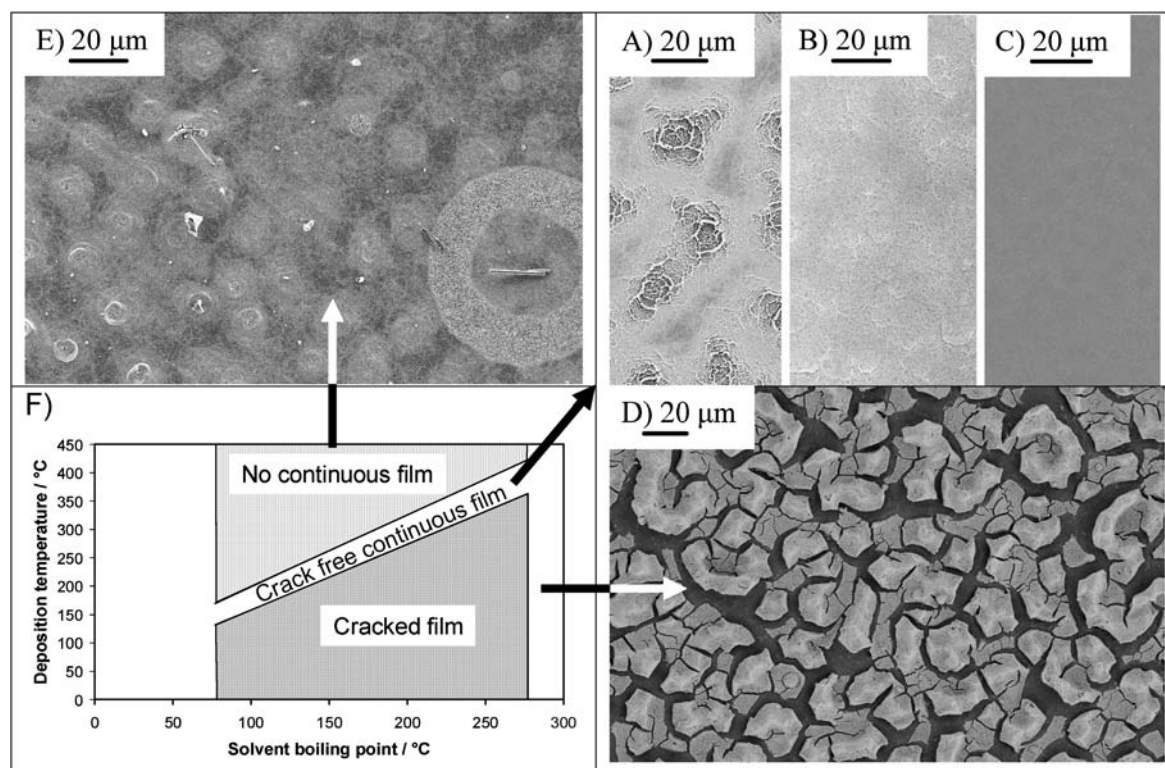


Fig. 3 A) to C): LSCF films deposited at $T_{\text{Deposition}}/T_{\text{SolventBoilingPoint}} = 1.16 \pm 0.01$ (in K), i.e. A) deposition at 255°C, solvent composition 1/3 ethanol, 2/3 diethylene glycol monobutyl ether (DGME); B) 225°C, 1/2 ethanol, 1/2 DGME; C) 195°C, 2/3 ethanol, 1/3 DGME. D) depo-

sition temperature 195°C, i.e. $T_{\text{dep}}/T_{\text{sbp}} = 1.02$, E) deposition at 320°C i.e. $T_{\text{dep}}/T_{\text{sbp}} = 1.31$. F) Schematic representation for the correlation between different morphologies, deposition temperature and solvent boiling point

The observation of faster film deposition at lower deposition temperature is widely reported in literature on spray pyrolysis [5, 14, 16]. This observation indicates that at this condition the droplets are still wet [6, 8, 17, 20, 25] when hitting the substrate. This means that at higher temperatures some of the small droplets are already dry and blown away from the film surface and do not contribute to the film formation. Instead of liquid droplets reaching the substrate a chemical vapor deposition (CVD) like process [22] where vapor reactants are responsible for film growth has also been proposed to explain film formation during spray pyrolysis. However because of the low temperatures ($<300^\circ\text{C}$) and the reported small evaporation rates during droplets transport [20, 30] this can not be the case in our experimental setup.

In most papers reporting on spray pyrolysis [1, 3, 5–8, 14, 16, 18–20, 22, 25, 28, 32–34], the substrate temperature during deposition is considered to be amongst the most critical parameters. However, the reported optimum temperature for crack-free films varies over a very wide range from 80°C [19] to about 500°C [3]. This is because the substrate temperature alone is not sufficient to determine the film quality. The decisive parameters are the drying and decomposition kinetics of the flying droplets and the growing film, which are in turn also determined by the solvent, the liquid and the gas flow rate, the material to be deposited, and the setup geometry.

As shown above, by just considering the ratio of deposition temperature (T_{dep}) to the solvent boiling point (T_{sbp}), one already gets an easy and effective “rule” for fabricating good films.

3.2. Salt concentration

Using a spray solution with a high salt concentration (0.04 mol/l) near the solubility limit, results in a rather smooth film as shown in Fig. 4A. If the salt concentration is lower (0.02 mol/l), the film shows a rougher surface, see Fig. 4B. In general, the roughness (Ra) measured for the case of low-salt concentration (0.02 mol/l) increases with deposition time from about $Ra = 0.15 \mu\text{m}$ for a 20 min deposition time to about $Ra = 0.25 \mu\text{m}$ for 90 min.

3.3. Solution flow rate

Spraying with the standard solution flow rate of 30 ml/h results in crack-free coherent films as already shown in Fig. 3A to C. Increasing the flow rate by a factor of two, results in cracked films. In this case the residual solvent content in the growing film is too high and leads to differential shrinkage and ultimately to crack formation. But when not

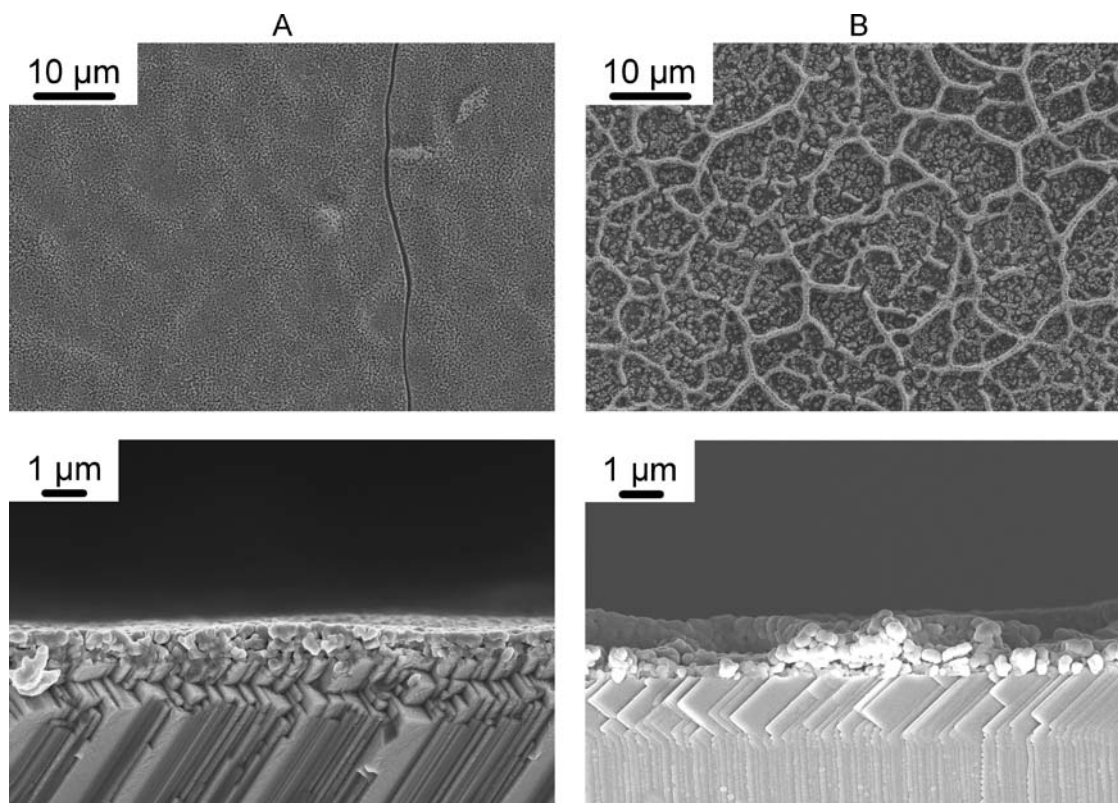


Fig. 4 Effect of different salt concentration. A) Higher salt concentration (0.04 mol/l) and shorter deposition times (30 min) lead to smoother films than in case B) with low salt concentration (0.02 mol/l) and longer

deposition times (60 min). Both: deposition temperature 275°C, annealing: 10 h @ 1000°C, 2 K/min

varied drastically, the flow rate has a minor importance in the spray process.

Perednis et al [7], also identified the solution-flow rate to have a minor influence on the film morphology, especially as long as a certain limit is not exceeded, which then would result in crack formation. Only one reference is found attributing a major role to the solution flow rate [12]. The authors report a significant change in microstructure from particle aggregates obtained at low solution-flow rates to a more layered structure obtained at high solution-flow rates. Unfortunately, no values are given for the two solution flow rates, thus the significance of this observation cannot be quantified.

3.4. Air pressure

Varying the air pressure results in a change of the droplet volume distribution as shown in Fig. 5A. Raising the pressure leads to a more uniform droplet volume distribution. The films shown so far (e.g. Fig. 3) are deposited at the standard pressure of 1 bar and do not show cracks. Fig. 5B to D shows a series of films deposited at the standard temperature but at different pressures: The film deposited at a lower pressure of 0.5 bar exhibits many cracks as shown in Fig. 5B. For an elevated pressure of 1.5 and 3 bar, as shown in Fig. 5C and D,

no cracks are found. On the contrary, with higher pressure, the film surface looks even smoother.

The change in droplet volume distribution with pressure is also confirmed by literature [6]. The air pressure influences also the drying kinetics during film deposition. Choosing low pressure leads to slower evaporation of the solvent in the droplet and results in a solvent rich film. Upon drying of the film, the differential shrinkage is too high thus cracks are formed. At elevated pressures, evaporation of the droplets is faster, hence the solvent content of the film is lower and cracks are avoided during drying of the film.

3.5. Model for film formation

Based on the results obtained, we suggest a model to describe the mechanisms and processes that take place during spray pyrolysis of the thin films. As shown schematically in Fig. 6, one can distinguish three basic situations. In the first case, shown in Fig. 6A, the ratio of $T_{\text{dep}}/T_{\text{sbp}}$ is low, i.e. in our case <1.15 . Starting from a clear solution, notable evaporation of the solvents occurs only in the last millimeters before the droplets hit the substrate [6, 20]. Due to the slow drying and decomposition kinetics obtained at low $T_{\text{dep}}/T_{\text{sbp}}$, only few particles precipitate in the droplet. The deposited film is thus a dilute suspension with a high solvent content. Thus the

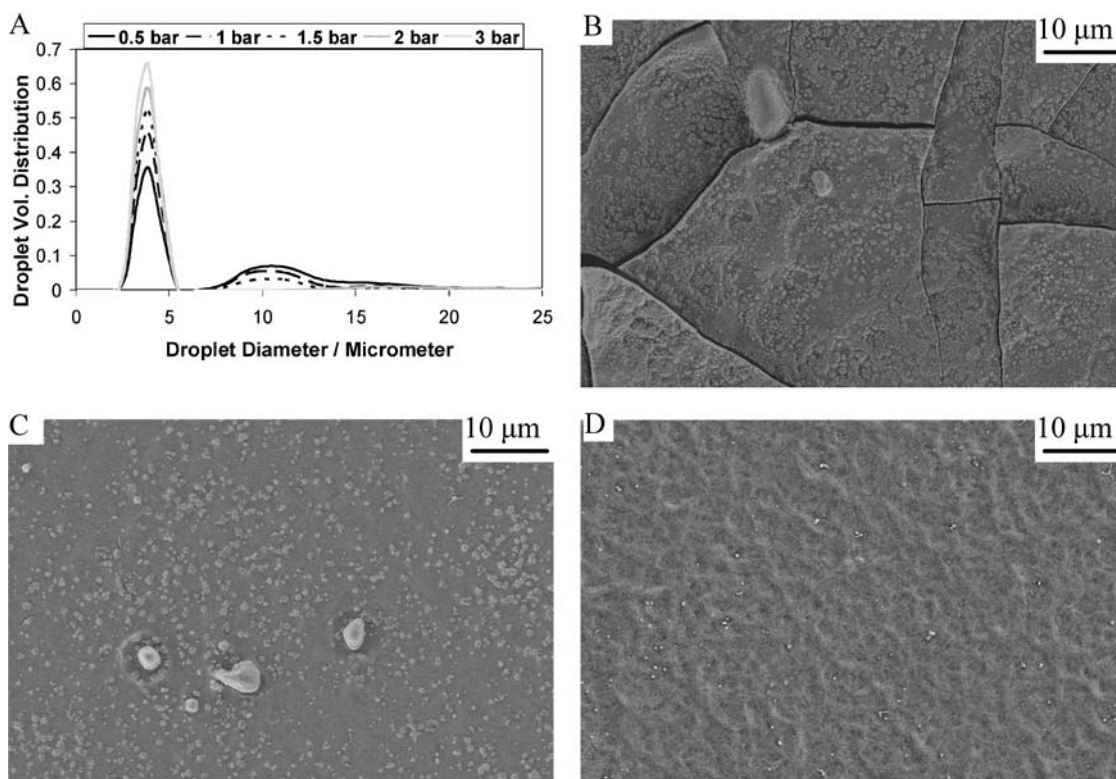


Fig. 5 A) Change of droplet volume distribution with pressure. As deposited LSCF films deposited with different air pressure: B) 0.5 bar, C) 1.5 bar, D) 3 bar. Total salt concentration in the solution: 0.04 mol/l, spraying time 30 min

differential shrinkage is so high that many cracks develop during drying as shown in Fig. 3D.

In the other extreme, shown in Fig. 6C for $T_{\text{dep}}/T_{\text{sbp}} > 1.25$, evaporation of the solvent is very fast, most droplets are already dry when reaching the substrate. Thus they do not stick to the substrate surface but are blown away and consequently they do not contribute to the film formation. Only few big droplets that are statistically formed at the nozzle will still reach the substrate in a wet state. However, since there are only few of these, they form isolated deposits, which do not cover the substrate continuously as shown in Fig. 3E.

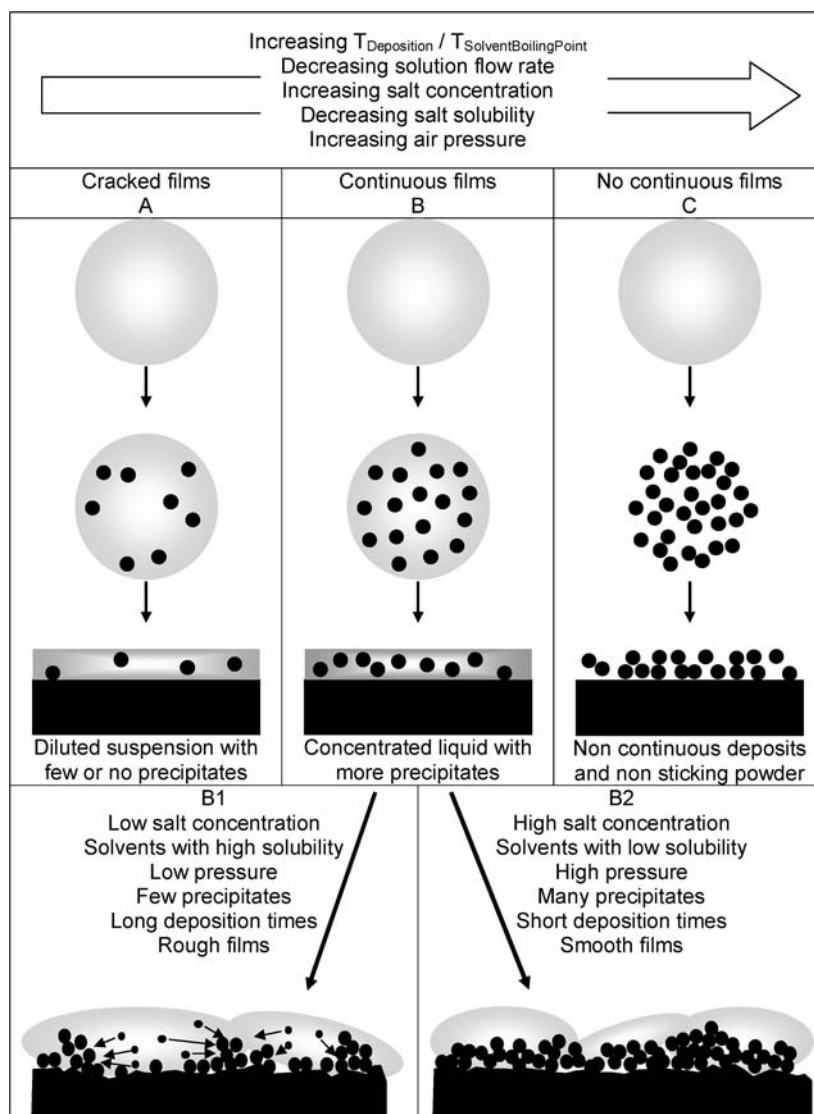
In the case, shown in Fig. 6B, a coherent crack-free film is obtained for $1.15 < T_{\text{dep}}/T_{\text{sbp}} < 1.25$. Depending on the exact conditions, the morphology and roughness varies. However, these details will be discussed later after the conditions to obtain coherent films are clarified. In case B, upon evaporation near the substrate, more particles precipitate than in case A. We consider formation of some precipitates in the droplets directly before or during impact on the substrate for the investigated system, because some of the solutions are at the solubility limit. A concentrated liquid containing many precipitates is obtained on the substrate. The residual solvent content is in this case sufficient to provide enough wetting of the substrate. On the other hand the solvent content is small enough to reduce differential shrinkage compared to case A.

Thus no cracks develop upon drying or annealing as shown in Fig. 3A to C.

Now the intermediate range $1.15 < T_{\text{dep}}/T_{\text{sbp}} < 1.25$ (case B) is discussed more closely. The first question is how the rough ridges on the film surface are formed (Fig. 3A), the second question is, why the morphology depends on the solvent composition. One possibility to form these ridges are capillary forces, which drag the solids load of a drying droplet to the edge of the droplet [38]. When comparing the amount of material carried by one droplet with the amount of material incorporated in one of these ridges, it can be calculated that due to the low solubility of the used salts, the material transported by one droplet is simply insufficient to build one of these ridges. Even a droplet which is more than twice as big (10 μm diameter) as the average droplet, carries 100 times less material than is required to build one of the smaller structures with a width and height of 1 μm and 10 μm diameter.

Therefore, we assume a different model: As schematically shown in Fig. 6B1 lateral movement of the droplet's content occurs upon impact on the substrate. The movement of the precipitates may be caused by the constant impact of new droplets on the substrate or by capillary forces. The important point is that the precipitates can move in the spreading and still wet droplets, until they hit an obstacle during their horizontal movement on the film surface. By this means, the

Fig. 6 Sketch of film formation, A) low $T_{\text{dep}}/T_{\text{sbp}}$ results in few precipitations, thus a diluted suspension is deposited, cracks form upon drying because of the high solvent content. B) Medium $T_{\text{dep}}/T_{\text{sbp}}$ results in a concentrated liquid with many precipitations. Depending on the conditions, B1) leads to rough films, B2) to smooth films. C) High $T_{\text{dep}}/T_{\text{sbp}}$ results in dry droplets, which lead to non continuous coverage of the substrate and powdery deposits that do not stick to the substrate



precipitates are constantly accumulated at rough obstacles, leading to the rougher films shown in Fig. 3A. If the concentration of the precipitates is higher as depicted in Fig. 6B2, the precipitates will obstruct each other and can not move over long distances. Thus, they stay where they randomly hit the substrate, forming smoother films as shown in Fig. 3C.

There are five possibilities to increase the number of precipitates: 1) using more of the worse solvent (ethanol) and less of the better solvent (diethylene glycol monobutylether). Thereby the saturation of salts in the solution is increased, leading to more precipitates. 2) Increasing the salt concentration also leads to smoother films due to more precipitates in the droplet. 3) Increasing the ratio $T_{\text{dep}}/T_{\text{sbp}}$ within the range for continuous crack-free film formation. 4) Decreasing the solution flow rate, thus less droplets share the same thermal energy for evaporation. 5) Increasing the air pressure, leads to

faster evaporation of the solvent and thus to more precipitates in the droplets.

We test the rule that coherent crack free films are obtained for $1.15 < T_{\text{dep}}/T_{\text{sbp}} < 1.25$ by also applying it to other systems: We can exchange some of the used nitrate salts by chlorides and vice versa and even replace the diethylene glycol monobutyl ether in the solvent by water and still obtain crack-free films. Although in this case the absolute substrate temperature is only 170°C . Furthermore we can also exchange some of the cations, e.g. replacing La by Ba, or spraying LSC only, or $\text{Sm}_{0.5}\text{Sr}_{0.5}\text{CoO}_3$ without a loss in film quality. For another setup geometry or very different liquid or gas flow rates, one may need to change the absolute numbers of the ratio $T_{\text{dep}}/T_{\text{sbp}}$, but knowing that this is the most important parameter, already simplifies the process of optimizing the spray pyrolysis parameters.

4. Summary

The most critical parameter when preparing thin films by spray pyrolysis is the ratio of deposition temperature to solvent boiling point, because it determines the drying and decomposition kinetics of the droplets and the growing film. For the investigated system, a ratio in the range of 1.15 to 1.25 (in K) proved to be useful. By keeping this ratio constant, the absolute deposition temperature could be varied by about 100°C, while still keeping a coherent crack-free film. Furthermore, the solvent, the salts, and some of the cations could also be exchanged without loss of film quality. Higher salt concentrations and the use of poor solvents during preparation of the spray solution lead to smoother films. Both parameters lead to stronger precipitation during evaporation of the droplets, which reach the substrate in a wet state. The more precipitates are present in the spreading droplets, the lower is their mobility because they obstruct each other and get stuck. Thus they stay where they randomly hit the substrate and form smooth films. The solution flow rate plays a minor role as long as it does not exceed a certain limit. The air pressure influences the drying kinetics. Higher pressure leads to faster drying and, furthermore, to a more uniform droplet distribution and smoother films. In the post deposition annealing step in air, a crystalline film of the desired perovskite phase is already obtained at 650°C having nano-sized grains.

Acknowledgments Financial support from Swiss BFE under the project OneBat—Start and KTI OneBat Discovery Project are gratefully acknowledged.

References

1. C.H. Chen, E.M. Kelder, P.J.J.M. van der Put, and J. Schoonman, *J. Mater. Chem.*, **6**(5), 765 (1996).
2. K. Choy, W. Bai, S. Charojrochkul, and B.C.H. Steele, *J. Power Sources*, **71**(1–2), 361 (1998).
3. T. Dedova, M. Krunk, O. Volobueva, and I. Oja, *Phys. Stat. Sol. (c)*, **2**(3), 1161 (2005).
4. C.-Y. Fu, C.-L. Chang, C.-S. Hsu, and B.-H. Hwang, *Mater. Chem. Phys.*, **91**(1), 28 (2005).
5. A. Furusaki, H. Konno, and R. Furuichi, *J. Mater. Sci.*, **30**(11), 2829 (1995).
6. D. Perednis, *Thin Film Deposition by Spray Pyrolysis and the Application in Solid Oxide Fuel Cells*, PhD Thesis, Swiss Federal Institute of Technology (Zurich, 2003).
7. D. Perednis, O. Wilhelm, S.E. Pratsinis, and L.J. Gauckler, *Thin Solid Films*, **474**(1–2), 84 (2005).
8. D. Perednis and L.J. Gauckler, *J. Electroceram.*, **14**(2), 103 (2005).
9. A. Princivalle, D. Perednis, R. Neagu, and E. Djurado, *Chem. Mat.*, **16**(19), 3733 (2004).
10. O. Stryckmans, T. Segato, and P.H. Duvigneaud, *Thin Solid Films*, **283**(1–2), 17 (1996).
11. M.S. Tomar and F.J. Garcia, *Prog. Cryst. Growth. Ch.*, **4**(3), 221 (1981).
12. P. Charpentier, P. Fragnaud, D.M. Schleich, C. Lunot, and E. Gehain, *Ionics*, **3**(1–2), 155 (1997).
13. L.D. Kadam and P.S. Patil, *Sol. Energy Mater.*, **69**(4), 361 (2001).
14. J. Morales, L. Sanchez, F. Martin, J. Ramos-Barrado, and M. Sanchez, *Thin Solid Films*, **474**(1–2), 133 (2005).
15. B.R. Pamplin, *Prog. Cryst. Growth. Ch.*, **1**(4), 395 (1979).
16. P.S. Patil, A.R. Patil, S.H. Mujawar, and S.B. Sadale, *J. Mater. Sci. Mater. El.*, **16**(1), 35 (2005).
17. S.H. Pawar, P.S. Patil, R.D. Madhale, and C.D. Lokhande, *Indian J. Pure Appl. Phys.*, **27**(5), 227 (1989).
18. D. Perednis and L.J. Gauckler, *Solid State Ionics*, **166**(3–4), 229 (2004).
19. T. Setoguchi, M. Sawano, K. Eguchi, and H. Arai, *Solid State Ionics*, **40–1**, 502 (1990).
20. O. Wilhelm, S.E. Pratsinis, D. Perednis, and L.J. Gauckler, *Thin Solid Films*, **479**(1–2), 121 (2005).
21. C.H. Chen, E.M. Kelder, and J. Schoonman, *J. Mater. Sci.*, **31**(20), 5437 (1996).
22. K.L. Choy and B. Su, *Thin Solid Films*, **388**(1–2), 9 (2001).
23. I. Taniguchi, R.C. van Landschoot, and J. Schoonman, *Solid State Ionics*, **156**(1–2), 1 (2003).
24. I. Taniguchi, R.C. van Landschoot, and J. Schoonman, *Solid State Ionics*, **160**(3–4), 271 (2003).
25. P. Bohac and L. Gauckler, *Solid State Ionics*, **119**(1–4), 317 (1999).
26. W.M. Sears and M.A. Gee, *Thin Solid Films*, **165**(1), 265 (1988).
27. L.D. Kadam, S.H. Pawar, and P.S. Patil, *Mater. Chem. Phys.*, **68**(1–3), 280 (2001).
28. P. Fragnaud, R. Nagarajan, D.M. Schleich, and D. Vujic, *J. Power Sources*, **54**(2), 362 (1995).
29. C.H. Chen, H.J.M. Bouwmeester, H. Kruidhof, J.E. tenElshof, and A.J. Burggraaf, *J. Mater. Chem.*, **6**(5), 815 (1996).
30. D. Perednis and L.J. Gauckler, In *8th International Symposium on Solid Oxide Fuel Cells*, edited by S.C. Singhal and M. Dokiya (The Electrochemical Society, Paris, 2003), 970.
31. D. Perednis, M.B. Joerger, K. Honegger, and L.J. Gauckler, In *7th International Symposium on Solid Oxide Fuel Cells*, edited by H. Yokokawa and S.C. Singhal (The Electrochemical Society, Tsukuba, 2001), 989.
32. C.M. Lampkin, *Prog. Cryst. Growth. Ch.*, **1**(4), 405 (1979).
33. G.L. Messing, S.C. Zhang, and G.V. Jayanthi, *J. Am. Ceram. Soc.*, **76**(11), 2707 (1993).
34. J.B. Mooney and S.B. Radding, *Annu. Rev. Mater. Sci.*, **81** (1982).
35. W.M. Yim and R.J. Paff, *J. Appl. Phys.*, **45**(3), 1456 (1974).
36. Mikrogilas, Material Properties of Foturan, www.mikrogilas.de, 2005.
37. J. ten Elshof and J. Boeijmsma, *Powder Diff.*, **11**(3), 240 (1996).
38. R.D. Deegan, O. Bakajin, T.F. Dupont, G. Huber, S.R. Nagel, and T.A. Witten, *Nature*, **389**(6653), 827 (1997).
39. G.C. Kostoglou and C. Ftikos, *Solid State Ionics*, **126**(1–2), 143 (1999).
40. Si, PDF 05–0565, JCPDS Database.